



This is a repository copy of *Imaging cellular trafficking processes in real time using lysosome targeted up-conversion nanoparticles*.

White Rose Research Online URL for this paper:
<http://eprints.whiterose.ac.uk/124987/>

Version: Accepted Version

Article:

Pramanik, S.K., Sreedharan, S., Singh, H. et al. (4 more authors) (2017) Imaging cellular trafficking processes in real time using lysosome targeted up-conversion nanoparticles. *Chemical Communications*, 94 (53). 12672-12675 . ISSN 1359-7345

<https://doi.org/10.1039/C7CC08185E>

Reuse

Items deposited in White Rose Research Online are protected by copyright, with all rights reserved unless indicated otherwise. They may be downloaded and/or printed for private study, or other acts as permitted by national copyright laws. The publisher or other rights holders may allow further reproduction and re-use of the full text version. This is indicated by the licence information on the White Rose Research Online record for the item.

Takedown

If you consider content in White Rose Research Online to be in breach of UK law, please notify us by emailing eprints@whiterose.ac.uk including the URL of the record and the reason for the withdrawal request.



eprints@whiterose.ac.uk
<https://eprints.whiterose.ac.uk/>

Imaging cellular trafficking processes in real time using lysosome targeted up-conversion nanoparticles

Received 00th January 20xx,
Accepted 00th January 20xx

DOI: 10.1039/x0xx00000x

Sumit Kumar Pramanik,^{[a]*} Sreejesh Sreedharan,^[b] Harwinder Singh,^[a] Carl Smythe,^[c] Jim. A. Thomas^{[b]*} and Amitava Das^{[a]*}

www.rsc.org/

β -NaYF₄:Yb,Gd up-conversion nanoparticles, UCNPs, surface functionalized with suitable targeting peptides function as nontoxic lysosome-specific imaging probes.

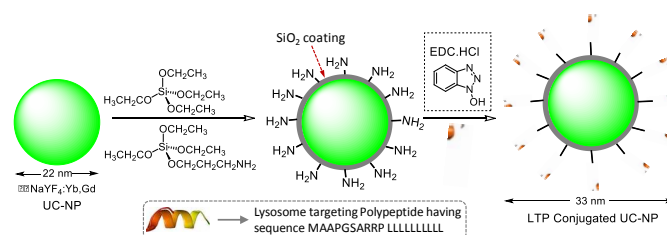
The lysosome is the cellular digestive organelle and contains key acid hydrolase enzymes.¹ Lysosomes also participate in intracellular signaling, energy metabolism, degradation of endocytosed and intracellular materials, and plasma membrane repair.^{1, 2} Defects in, or alteration of, lysosomal structure and function is associated with multiple pathologies, including inflammation, several types of cancer, neurodegenerative diseases, immune-deficiency diseases, pigmentation-bleeding disorders and specific lysosomal storage diseases such as TaySachs.³⁻⁶ Currently, there is no direct medical treatment to cure lysosomal storage diseases, and - due to their intrinsic complexity - investigations into endo-lysosomal activity present a major research challenge.⁷ For this reason, lysosome targeted imaging agents are crucial in real-time probing of this organelle's role in intracellular processes.^{6, 8, 9}

Though fluorescence imaging is a useful tool in visualizing the localization, dynamics of specific biomolecules and biochemical transformations,¹⁰⁻¹² molecular fluorescent probes often suffer from problems such as interference from nonspecific background emission, high photo-bleaching rates, and cytotoxicity. Some of these problems may be addressed through the development of organelle-specific fluorescent probes, which could also offer applications as potential diagnostics.²⁰⁻²²

As imaging agents, quantum dots (QDs) offer bright photoluminescence, high quantum yields, broad ultraviolet

excitation, and high photostability.^{10, 11} However, QDs are often chemically unstable and can be highly toxic.¹¹ In this context, lanthanide-based up-converting phosphors (UCPs) offer some distinct advantages: they possess narrow emission bands that suppress scattering, have tuneable emissions with long luminescent lifetime, display large Stokes and anti-stokes shift. They are also chemically and photochemically stable, and exhibit low toxicity.¹²⁻¹⁶ As photon upconversion systems they can be excited with near-infrared (NIR), which helps in suppressing interference from endogenous background fluorescence. This factor along with their low scattering, helps them to achieve high signal-to-noise ratios in imaging.¹⁴

At the same time, small peptides have become key components in the surface functionalization of nanostructures for biological application, This is due to their inherent biocompatibility, ease of synthesis and diversity of function^{17, 18} Previous reports have revealed that peptide-conjugated nanoparticles can be used to target subcellular structures and thus provide potential application as drug-delivery systems.¹⁹⁻²² Cell-penetrating peptides, CPPs, can cross the cellular membrane and transport bioactive cargoes to specific cellular organelles such as nuclei, lysosomes or mitochondria in a nontoxic and efficient way.^{23, 24}



Scheme 1. Schematic presentation for the development of LTP-Conjugated UC-NP.

Earlier studies confirm that hexagonal β -phase NaYF₄ is an excellent up-converting host material ($\lambda_{\text{Ext}} = 980 \text{ nm}$) and can be doped with Yb-Er or Yb-Tm or Y-Ho rare-earth ion couples for various optical applications.^{25, 26} Although, β -NaYF₄:Yb,Er/Tm/Ho UC-NPs have been used for the detection of avidin, DNA and in imaging cells and tissues, use of such material in specific subcellular organelle imaging is still rare.

^a CSIR-Central Salt & Marine Chemicals Research Institute, Bhavnagar: 364002, Gujarat, India; E-Mail: sumitpramanik@csmcri.res.in (SKP); a.das@csmcri.res.in (AD)

^b Department of Chemistry, University of Sheffield, Sheffield, S3 7HF, UK, Email: james.thomas@sheffield.ac.uk (JAT).

^c Department of Biomedical Science, University of Sheffield, Sheffield, S10 2TN, UK. [†] equally contributing to this work.

Electronic Supplementary Information (ESI) available: [details of any supplementary information available should be included here]. See DOI: 10.1039/x0xx00000x

In this study, we explored the possibility of using lysosomal targeting peptide (LTP), a C-terminal 20-residue sequence from the lysosome-associated membrane glycoprotein, for surface functionalization of NaYF₄:Yb,Gd UC-NPs and thus achieving lysosome specific imaging reagent with low cytotoxicity and high cellular uptake – Scheme 1. The sequence of LTP, used for our studies, is MAAPGSARRP LLLLLLLLLL, where the N-terminal is protected with biotin and the C-terminal of leucine is available for facile conjugation to the UC-NPs.²⁷

NaYF₄:Yb,Gd UC-NPs with uniform size were synthesized by hydrothermal reaction (SI). The synthesized nanoparticles were fully characterized by powder X-ray diffraction (XRD), transmission electron microscopy (TEM), Fourier transform infrared spectroscopy (FT-IR), and dynamic light scattering (DLS). Subsequently, following a typical Stöber-based surface modification, primary amino groups were introduced onto their surface, allowing chemical coupling between the UC-NPs and LTP.

The phase purity, crystallinity and composition of the synthesized β -NaYF₄:Yb,Gd UC-NPs was determined by powder XRD. The powder-XRD pattern of the synthesized UC-NPs (Fig. S1, ESI†) exhibits sharp diffraction peaks that are indexed to pure hexagonal-phase β -NaYF₄ (JCPDS No. 0281192; space group: P63/m).²⁸ The absence of other phases indicates the high purity of the synthesized UC-NPs, while the sharpness of the peaks indicates higher crystallinity for β -NaYF₄:Yb,Gd UC-NPs. This lack of trap sites leads to high luminescence yields.

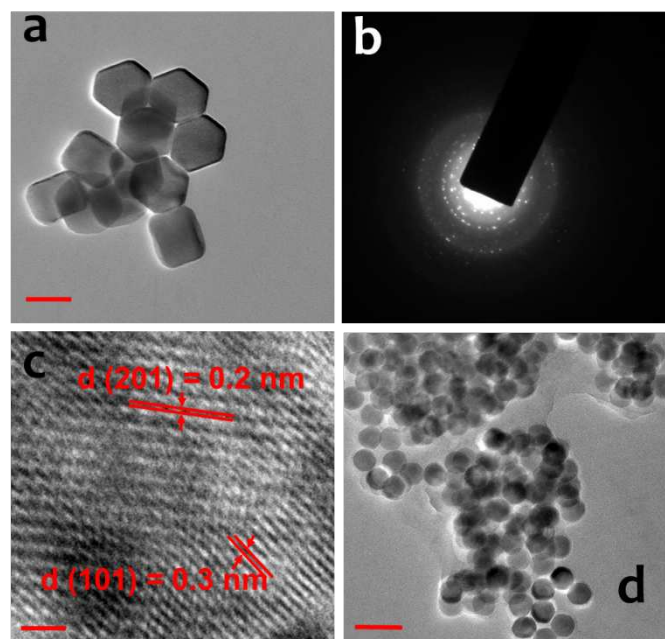


Fig. 1 TEM images of (a) β -NaYF₄:Yb,Gd NPs; (b) and (c) are corresponding SAED patterns and HRTEM images of β -NaYF₄:Yb,Gd NPs; (d) LTP-conjugated β -NaYF₄:Yb,Gd NPs. The UC-NPs are highly crystalline and well-separated even after LTP conjugation.

The size and morphology of the β -NaYF₄:Yb,Gd UC-NPs were characterized by TEM and DLS studies. Typical TEM image, shown in Fig. 1a, reveal hexagonal, well-dispersed particles with a uniform diameter of \sim 22 nm. The selected area electron diffraction pattern (SAED) (Fig. 1b) and high-resolution TEM

images (Fig. 1c) confirms the highly crystalline nature of the synthesized UC-NPs. Lattice fringes with inter-planar spacing of 0.3 nm are attributed to the (101) planes of NaYF₄:Yb,Gd.²⁹ Energy dispersive X-ray analysis confirms the elemental composition and the presence of Y, Si, Yb and Gd (Fig. S2, ESI†). TEM images of UC-NPs surface functionalized with LTP reveal an increase in the average size to about 11 nm (Figure 2d) without any apparent change in their shape and size monodispersity (Fig. 1d and Fig. S3, ESI†).

A closer look at the DLS data reveals a distinct increase in the hydrodynamic diameters of the particles from (29.8 \pm 2.0) nm for NaYF₄:Yb,Gd UC-NPs to (47.5 \pm 1.5) nm for LTP conjugated UC-NPs. The initial zeta potential of (38 \pm 0.5) mV for NaYF₄:Yb,Gd NPs decreases significantly to (-24.9 \pm 0.4) nm after surface functionalization of UC-NPs with LTP. This change is attributed to the pronounced hydration of the peptide in the aqueous phase. Thus, DLS measurements and TEM characterization unambiguously confirm peptide conjugation onto the amino-modified NaYF₄:Yb,Gd NPs.

The functional groups on the surfaces of bare and amino-modified NaYF₄:Yb,Gd NPs were confirmed by FT-IR spectroscopy. The surfaces of the bare NPs are coated with a layer of hypermer B246, which acts as the surfactant as well as the capping ligand during the synthesis. The stretching vibration of hydroxyl group of hypermer B246 exhibits a broad transmission band at around 3250 cm⁻¹ (Fig. 2a).³⁰ FT-IR spectra of the amino-modified NaYF₄:Yb,Gd NPs reveal bands at 3434 cm⁻¹ (broad) and 1608 cm⁻¹ for N-H stretching and N-H bending vibrations, respectively. The symmetrical stretching vibration of Si-O bond appears at 1103 cm⁻¹. Moreover, two peaks at 2921 and 2847 cm⁻¹ are assigned to the asymmetric and symmetric stretching vibrations of methylene group of 3-aminopropyltriethoxysilane. For LTP conjugated UC-NPs, a stretching vibration band at 1658 cm⁻¹ (Figure 3c) is observed, this is assigned to -C=O amide bond formation through the reaction between the amine group of UC-NPs and the carboxyl group of C-terminal LTP.

The upconversion photoluminescence spectra of the synthesized LTP conjugated UC-NPs was recorded following excitation with a 980 nm laser source (Fig. 2b). The green emission band at around 525 - 560 nm can be assigned to electronic transitions from ²H_{11/2} \rightarrow ⁴I_{15/2} and ⁴S_{3/2} \rightarrow ⁴I_{15/2}.

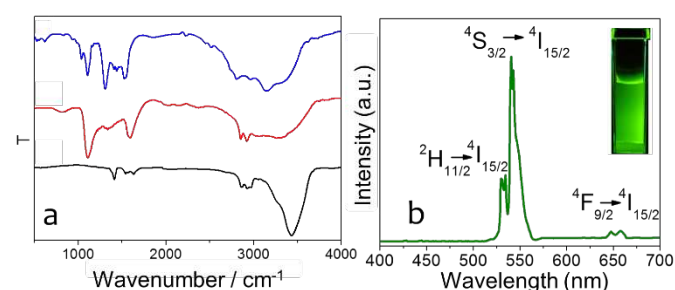


Fig. 2 (a) The FT-IR spectra of bare NPs (black); silica coated β -NaYF₄:Yb,Gd NPs (red) and LTP conjugated UC-NPs (blue). (b) Up conversion fluorescence spectra of solid LTP appended NaYF₄:Yb,Gd NPs. Inset is the photograph of 0.5 wt % colloidal solution of resultant NPs in water, excited with a 980 nm laser.

While, the red emission band at around 640 - 660 nm is attributed to a $^4F_{9/2} \rightarrow ^4I_{15/2}$ transition of the Yb^{3+} ions of $\text{NaYF}_4:\text{Yb,Gd}$. Here, first Yb^{3+} absorbs 980 nm wavelength light and consequently transfers this energy to a nearby Gd^{3+} ion, exciting Gd^{3+} to the $^4I_{11/2}$ level. After that a second 980 nm photon from an excited Yb^{3+} can populate the $^4F_{7/2}$ level of Gd^{3+} , which then relaxes non-radiatively to the $^2H_{11/2}$ and $^4S_{3/2}$ levels. This results in green (520 nm, $^2H_{11/2} \rightarrow ^4I_{15/2}$; 540 nm, $^4S_{3/2} \rightarrow ^4I_{15/2}$) and red (654 nm, $^4F_{9/2} \rightarrow ^4I_{15/2}$) emissions, respectively.³¹

Results of our imaging studies reveals that bare $\text{NaYF}_4:\text{Yb,Gd}$ UC-NPs are not an efficient imaging reagent due to their low cellular uptake and lack of any organelle specificity. This is further corroborated by reports on analogous UC-NPs.³² Given that $\text{NaYF}_4:\text{Yb,Gd}$ NPs are well-established optical upconversion systems, the suitability of the new systems for two photon microscopy, TPM, was also assessed (Fig. 3). Using this technique, intense intracellular emission signals were observed. TPM images show that the UC-NPs are taken up by cells, displaying bright luminescence within the cytosol, Fig. 3a. An increase in the treatment concentration of UC-NPs also produces a concomitant increase in intracellular emission, Fig. 3b. This is also evident in the intensity maps generated from these data, Fig. 3c. The images show that luminescence is almost entirely from the cytoplasmic region with negligible emission observed from the nucleus. The punctuated nature of the images, which is observed in the intensity maps (Fig. 3c), also indicates that the UC-NPs localize in specific regions within the cytoplasm. This was investigated in more detail through co-localization studies.

Since UC-NPs are decorated with LTP, the possibility that the nanoparticles are delivered to lysosomes was explored with the help of Lyso Tracker Deep Red, LTDR, whose spectral properties are complementary to those of the nanoparticles; the NPs are one-photon excited at 488 nm and their emission is collected at 500 to 550 nm, whereas LTDR is excited at 644 nm and emits at 655 nm (Fig. 4).

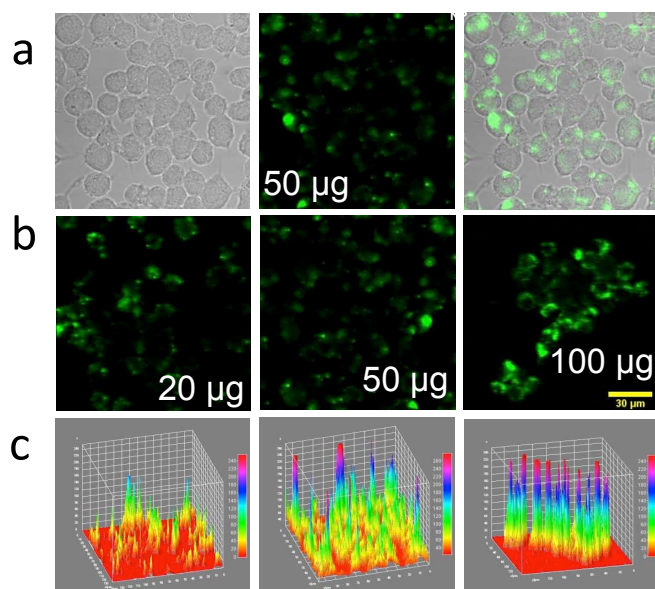


Fig. 3 Optical microscopy images showing uptake of UC-NPs (A) Phase contrast (left), emission after two photon absorption (middle), combined image (right) of RAW cells. B. Effect of increasing concentration of UCP-NP treatment: 20 μg (left), 50 μg (middle), 100 μg (right). C. Intensity maps for the same concentrations shown in B. (Pseudo colour has been employed in all the images). $\lambda_{\text{exc}} = 975 \text{ nm}$.

The intensity profile of the Widefield images indicates that 40 percent of the signals of Lyso Tracker Deep Red matches with that of the LTP-conjugated UC-NPs. The calculated Pearson's coefficient (82%) also supports the supposition that NPs are localized in the lysosomes of RAW cells (Fig. 4). For further confirmation of subcellular localization, similar co-localization experiments, with Mito Tracker Deep Red (MTDR) and Hoechst 33258, were performed. Fig. S4 and Fig. S5 (ESI[†]). These studies confirm that the nanoparticles do not localise in mitochondria nor nuclei, confirming that the LTP conjugated $\text{NaYF}_4:\text{Yb,Gd}$ UC-NPs are exclusively lysosome targeting.

Biocompatibility studies using the MTT assay performed on redispersed LTP conjugated UC-NPs showed that viability levels in treated cells remained stable compared to a control group. Indeed, no decrease below 99 % was observed even after exposures to different concentrations of LTP conjugated UC-NPs of up to 24 hrs (Fig. S7, ESI[†]). This confirms that the nanoprobe are fully biocompatible, making them excellent candidates for biomedical applications.

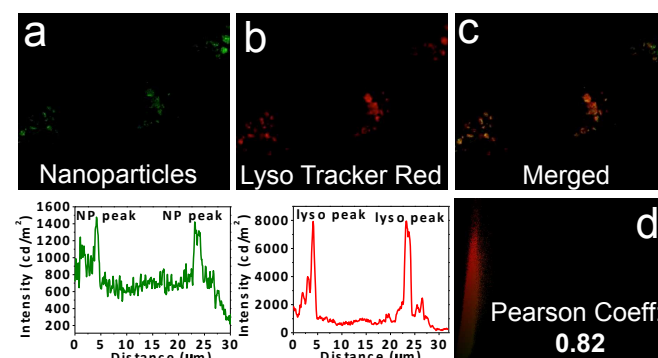


Fig. 4 Colocalization experiments of Intracellular localization of UC-NPs using Lyso Tracker probes: Wide field microscopy images of in cellulo emission of UC-NPs (Panel a) with intensity along traced line shown underneath. Emission from Lyso Tracker Deep Red (Panel b) and intensity along the same line shown below. The overlap of the intensity is shown in Panel c. Panel c shows the overlap of the green and red fluorescence, indicating lysosomal localization of the UC-NPs. Panel d shows the Pearson co-efficient = 0.82.

In conclusion, a two photon excitable composite nanoprobe has been developed. To the best of our knowledge, this is the first report on surface modification of UC-NPs with an organelle targeting peptide to transform inorganic nanoparticles into organelle specific two photon imaging nanoprobe. These lysosome targeting UC-NPs may offer application in the study of intracellular transport mechanisms and lysosome-based diseases. It is envisaged that this approach to surface chemistry can be extended to develop other subcellular imaging nanoprobe and future studies will extend the possibilities of using such systems for *in-vivo* imaging technologies which may provide potential applications in areas such as fluorescence-guided surgery.

Acknowledgement

A.D. acknowledges SERB (India) (SB/S1/IC-23/2013 & JCB/2017/000004) and DRDO (ERIP/ER/1502249/M/01) Grants for funding. SKP acknowledge SERB (India) Grant PDF/2015/000745 for funding and fellowship. HS acknowledges DRDO Grant (ERIP/ER/1502249/M/01) for a research fellowship. SS and JAT are grateful to the Imaging Life initiative of the University of Sheffield, and MRC funding for the SIM facilities.

Conflicts of interest

There are no conflicts to declare.

Notes and references

1. K. Rae Chi, *Nature*, 2016, **537**, S148-S150.
2. F. M. Platt, *Nature*, 2014, **510**, 68-75.
3. H. Maes and P. Agostinis, *Mitochondrion*, 2014, **19**, Part A, 58-68.
4. Z. Chen, H. Yuan and H. Liang, *ACS Applied Materials & Interfaces*, 2017, **9**, 9260-9264.
5. A. Abeliovich and A. D. Gitler, *Nature*, 2016, **539**, 207-216.
6. R. M. Perera, S. Stoykova, B. N. Nicolay, K. N. Ross, J. Fitamant, M. Boukhali, J. Lengrand, V. Deshpande, M. K. Selig, C. R. Ferrone, J. Settleman, G. Stephanopoulos, N. J. Dyson, R. Zoncu, S. Ramaswamy, W. Haas and N. Bardeesy, *Nature*, 2015, **524**, 361-365.
7. L. Yu, C. K. McPhee, L. Zheng, G. A. Mardones, Y. Rong, J. Peng, N. Mi, Y. Zhao, Z. Liu, F. Wan, D. W. Hailey, V. Oorschot, J. Klumperman, E. H. Baehrecke and M. J. Lenardo, *Nature*, 2010, **465**, 942-946.
8. D.-Y. Zhang, Y. Zheng, C.-P. Tan, J.-H. Sun, W. Zhang, L.-N. Ji and Z.-W. Mao, *ACS Applied Materials & Interfaces*, 2017, **9**, 6761-6771.
9. W. Zhang, Y. Ji, X. Wu and H. Xu, *ACS Applied Materials & Interfaces*, 2013, **5**, 9856-9865.
10. J. P. Park, J.-J. Lee and S.-W. Kim, *Scientific Reports*, 2016, **6**, 30094.
11. Y. Wang and A. Hu, *Journal of Materials Chemistry C*, 2014, **2**, 6921-6939.
12. Y. Li, S. Zhou, G. Dong, M. Peng, L. Wondraczek and J. Qiu, *Scientific Reports*, 2014, **4**, 4059.
13. X. Wu, G. Chen, J. Shen, Z. Li, Y. Zhang and G. Han, *Bioconjugate Chemistry*, 2015, **26**, 166-175.
14. X. Zhu, Q. Su, W. Feng and F. Li, *Chemical Society Reviews*, 2017, **46**, 1025-1039.
15. Y. Liu, Y. Lu, X. Yang, X. Zheng, S. Wen, F. Wang, X. Vidal, J. Zhao, D. Liu, Z. Zhou, C. Ma, J. Zhou, J. A. Piper, P. Xi and D. Jin, *Nature*, 2017, **543**, 229-233.
16. X. Xie, F. Tang, X. Shangguan, S. Che, J. Niu, Y. Xiao, X. Wang and B. Tang, *Chemical Communications*, 2017, **53**, 6520-6523.
17. I. Adipurnama, M.-C. Yang, T. Ciach and B. Butruk-Raszeja, *Biomaterials Science*, 2017, **5**, 22-37.
18. O. Veisoh, J. Gunn and M. Zhang, *Advanced drug delivery reviews*, 2010, **62**, 284-304.
19. A. G. Tkachenko, H. Xie, D. Coleman, W. Glomm, J. Ryan, M. F. Anderson, S. Franzen and D. L. Feldheim, *Journal of the American Chemical Society*, 2003, **125**, 4700-4701.
20. P. Nativo, I. A. Prior and M. Brust, *ACS Nano*, 2008, **2**, 1639-1644.
21. C. D. Dekiwadia, A. C. Lawrie and J. V. Fecondo, *Journal of Peptide Science*, 2012, **18**, 527-534.
22. J. Conde, A. Ambrosone, V. Sanz, Y. Hernandez, V. Marchesano, F. Tian, H. Child, C. C. Berry, M. R. Ibarra, P. V. Baptista, C. Tortiglione and J. M. de la Fuente, *ACS Nano*, 2012, **6**, 8316-8324.
23. K. M. Stewart, K. L. Horton and S. O. Kelley, *Organic & Biomolecular Chemistry*, 2008, **6**, 2242-2255.
24. D. M. Copolovici, K. Langel, E. Eriste and Ü. Langel, *ACS Nano*, 2014, **8**, 1972-1994.
25. G. Chen, H. Qiu, P. N. Prasad and X. Chen, *Chemical Reviews*, 2014, **114**, 5161-5214.
26. W. Zheng, P. Huang, D. Tu, E. Ma, H. Zhu and X. Chen, *Chemical Society Reviews*, 2015, **44**, 1379-1415.
27. L. D. Field, J. B. Delehanty, Y. Chen and I. L. Medintz, *Accounts of Chemical Research*, 2015, **48**, 1380-1390.
28. Q. Chen, X. Wang, F. Chen, Q. Zhang, B. Dong, H. Yang, G. Liu and Y. Zhu, *Journal of Materials Chemistry*, 2011, **21**, 7661-7667.
29. P. Padhye, A. Alam, S. Ghorai, S. Chattopadhyay and P. Poddar, *Nanoscale*, 2015, **7**, 19501-19518.
30. S. Kuypers, S. K. Pramanik, L. D'Olieslaeger, G. Reekmans, M. Peters, J. D'Haen, D. Vanderzande, T. Junkers, P. Adriaensens and A. Ethirajan, *Chemical Communications*, 2015, **51**, 15858-15861.
31. R. Wang and F. Zhang, in *Near-infrared Nanomaterials: Preparation, Bioimaging and Therapy Applications*, The Royal Society of Chemistry, 2016, DOI: 10.1039/9781782623939-00001, pp. 1-39.
32. S. F. Lim, R. Riehn, W. S. Ryu, N. Khanarian, C.-k. Tung, D. Tank and R. H. Austin, *Nano Letters*, 2006, **6**, 169-174.